Thermodynamic and stoichiometric stability of the Cd-terminated CdTe (111) surface

Jin Li,[1] Nicholas Kioussis,[1] F. Aqariden,[2] and C. Grein[2]
[1]*Department of Physics, California State University, Northridge, California 91330-8268, USA*
[2]*Sivananthan Laboratories, 590 Territorial Dr, Unit H, Bolingbrook, Illinois 60440, USA*
(Received 12 March 2012; published 11 June 2012)

Employing *ab initio* thermodynamics calculations, we elucidate for the first time the effects of growth conditions on the reconstruction phase diagram of the polar Cd-terminated CdTe (111) surface and resolve an existing experimental controversy of the low-temperature reconstruction under Te-rich conditions. We demonstrate that the Cd-vacancy (2×2) reconstruction is the most stable configuration in the allowed range of the Te chemical potential. Under Te-rich conditions, however, the calculations reveal a transition from a high-temperature semiconducting (2×2) to a low-temperature metallic (1×1)-Te$_n$ reconstruction consisting of n Te adlayers forming a spiral trigonal structure. We also predict the temperature and pressure dependence of the Te thickness adlayer, which has remained experimentally unresolved.

DOI: 10.1103/PhysRevB.85.235306 PACS number(s): 68.35.−p, 68.43.−h, 73.20.At

I. INTRODUCTION

Among the various II-VI semiconductor materials, cadmium telluride (CdTe) and CdTe-based alloys continue to attract a great deal of interest because they combine both fascinating fundamental physics and a wide spectrum of important technological applications. CdTe is an important thin-film solar-cell material due to its 1.5 eV direct band gap, which is near the optimum for conversion efficiency in a single-junction solar cell under terrestrial irradiation.[1,2] CdZnTe is the most promising material for x-ray and gamma-ray detectors due to its high atomic number, wide band gap, high detection efficiency of high-energy photons, and high mobility and lifetime of charge carriers.[1,3] The $Hg_{1-x}Cd_xTe$ alloys have become the material of choice for many high-performance infrared detection applications because they offer band-gap tunability with alloy concentration through nearly the entire infrared spectrum.[4] Recently, the CdTe/HgTe quantum well has sparked great interest due to theoretical predictions[5] and subsequent experiments[6] which revealed a quantum phase transition from a normal to a topological insulator upon varying the quantum well thickness.

In all these applications, besides the quality of the bulk crystal, the quality of the CdTe surfaces and interfaces are often the dominant factors influencing the device performance.[7] The polar CdTe (111) surface with Cd-terminated (111) A surface or Te-terminated $(\bar{1}\bar{1}\bar{1})$ B surface is of particular technological importance for the epitaxial growth of II-VI compounds. Various surface treatments, such as sputtering, annealing, and mechanical and chemical processing, change the surface morphology and induce various defects, affecting in turn the electronic structure and hence the transport properties. Depending on the crystal growth conditions, the Cd-terminated surface undergoes different reconstructions which remain controversial.

X-ray photoelectron spectroscopy (XPS) and reflection high-energy electron diffraction (RHEED)[8–10] of the molecular-beam epitaxy (MBE)-grown A surface have shown that at temperatures $\geqslant$320 °C the cation-terminated surface displays a (2×2) reconstruction. On the other hand, the low-temperature structure remains controversial. At temperatures $\leqslant$120 °C the (1×1) reconstruction is observed, consisting of several Te monolayers (ML), which is stable only under Te-rich conditions.[9,10] For example, at 230 °C the (1×1) reconstruction undergoes a transition to a (2×2) reconstruction if the Te flux is less than 3×10^{-7} Torr.[10] Low-energy electron diffraction (LEED) has also observed the Te-covered (1×1) reconstruction for clean surfaces prepared using 600 eV Ar^+ sputtering and annealing at ∼250 °C.[11] In sharp contrast, using similarly prepared samples and an 800 eV Ar^+ beam Gordon *et al.* found[12] that the (111) A surface is unreconstructed. On the other hand, employing Ar^+ sputtering with a higher beam energy of 1 keV, recent scanning tunneling microscopy (STM) experiments observed only the (2×2) reconstruction.[13] Interestingly, the (111) A surface of $Cd_{0.96}Zn_{0.04}Te$ alloys exhibits a $(\sqrt{3} \times \sqrt{3})R30°$ reconstruction.[14] Thus, the experimental studies raise several intriguing questions regarding the effect of growth conditions on the atomic and electronic structure of the CdTe (111) A surface.

In this work, we present for the first time a comprehensive study of the effects of growth conditions on the reconstruction phase diagram of the CdTe (111) A surface employing *ab initio* thermodynamics calculations.[15,16] We find that the Cd-vacancy (2×2) reconstruction is energetically favorable over all other candidate structures in the allowed range of Te chemical potential. Under Te-rich conditions, however, the calculations reveal a transition from the semiconducting (2×2) to the metallic (1×1)-Te$_n$ reconstruction consisting of n Te ML over the Cd-terminated surface, in agreement with experiments.[10,11] We also derive a general expression of the temperature and pressure dependence of the Te adlayer thickness, which remains experimentally unresolved.

II. METHODOLOGY

The density functional theory calculations employed the Vienna Ab initio Simulation Package (VASP)[17], with the projector-augmented-wave[18] approach and the local density approximation.[19] The Cd 4*d* electrons are treated explicitly as valence electrons. The (111) A surface is modeled by a periodic slab consisting of 12 atomic layers and a 16-Å-thick vacuum region separating the periodic slabs. The bottom Te layer is passivated by pseudohydrogen atoms. The atomic

positions of the top eight atomic layers were fully relaxed using the conjugate gradient algorithm until all interatomic forces are smaller than 0.01 eV/nm. The energy cutoff of the plane-wave expansion of the basis functions was set to be 475 eV. The Brillouin-zone (BZ) integration was performed using the $11 \times 11 \times 1$, $7 \times 7 \times 1$, and $5 \times 5 \times 1$ k-point mesh[20] for the (1×1), $(\sqrt{3} \times \sqrt{3})$R30°, and (2×2) reconstructions, respectively. Test calculations with a larger cutoff energy of 600 eV and denser k-point mesh confirmed convergence of the surface free energies of the various reconstructions smaller than 0.5 meV/Å^2.

We have considered the unreconstructed (1×1), the reconstructed (2×2),[13] $(\sqrt{3} \times \sqrt{3})$R30°,[14] and the (1×1)-Te$_n$ consisting of $n = 1$–9 Te MLs above the Cd-terminated surface shown in Fig. 1. For the (1×1)-Te$_1$ single ML reconstruction, we examined Te atoms adsorbed on the hcp hollow site, (1×1)-Te$_1$-adatom(hcp), and atop sites above the Cd, (1×1)-Te$_1$-adatom(Cd), and Te (1×1)-Te$_1$-adatom(Te) surface atoms, respectively.

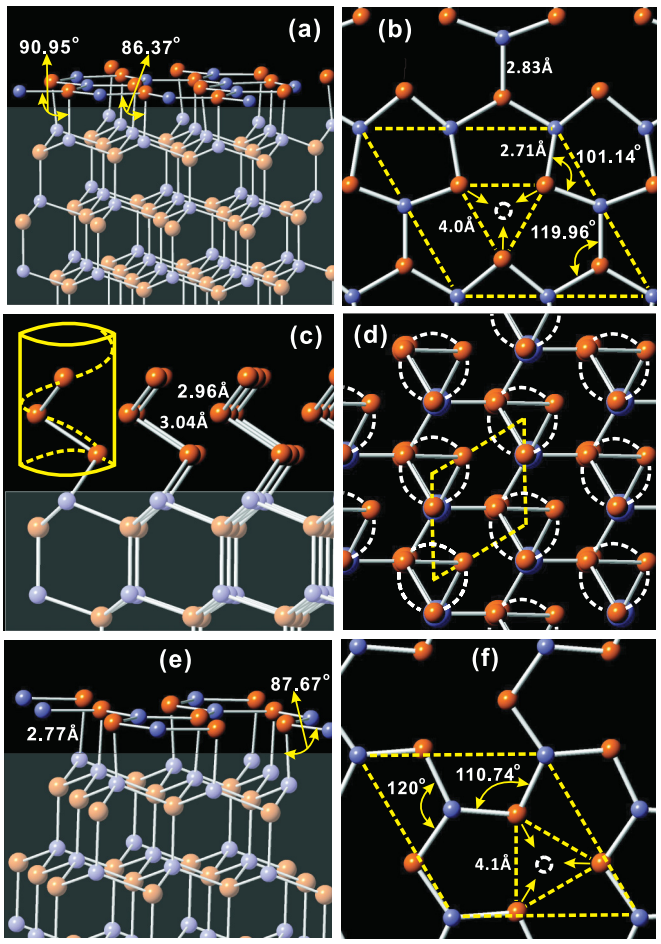

FIG. 1. (Color online) Side views [left panels (a), (c), and (e)] and top views [right panels (b), (d), and (f)] of the (2×2), (1×1)-Te$_3$, and $(\sqrt{3} \times \sqrt{3})$R30° reconstructions of the CdTe (111) A surface, respectively. The blue (red) circles denote the Cd (Te) atoms, and the white dashed circle denotes the Cd surface vacancy. The shaded region denotes all ML except for the surface. Panel (b) shows the unit cell of the spiral trigonal structure of the Te overlayer consisting of helices normal to the surface with three atoms per turn.

The thermodynamic stability of various surface structures in the constant pressure and temperature ensemble can be determined from the surface free energy,[15,16]

$$\gamma(T,p,N_i) = \frac{1}{A}\left[G^{\text{surf}}(T,p,N_i) - \sum_i N_i \mu_i(T,p)\right], \quad (1)$$

where G^{surf} is the Gibbs free energy of the surface, N_i is the number of the ith type of atoms, $\mu_i(T,p)$ is the chemical potential of the ith atomic species at temperature T and pressure p, and A is the surface area. The contributions of the configurational free energy F_{conf} and pV to the free energy are negligible and hence are neglected, as in previous studies.[16] Using the Einstein model for the phonon density of states and the average vibrational frequency, we find that the vibrational contribution to the surface free energy is rather small (about 1 meV/Å^2) and can not change the surface phase diagram. Therefore, the vibrational contributions have not been included in the present work. Even though the kinetics of growth processes have been neglected, the thermodynamic approach of Gailliard provides[21] a correct description of the MBE growth if the kinetics are fast enough to ensure partial local equilibrium across the growth surface.

The temperature and pressure dependence of the chemical potential of Te$_2$ in the vapor phase is

$$2\mu_{Te}(T,p) = E_{Te_2} + k_B T\left[\ln\left(\frac{pV_Q}{k_B T}\right) - \ln Z_{\text{rot}} - \ln Z_{\text{vib}}\right], \quad (2)$$

where E_{Te_2} is the energy of a Te molecule, k_B is the Boltzmann constant, $V_Q = (h^2/2\pi m k_B T)^{3/2}$, and Z_{rot} and Z_{vib} are the rotational and vibrational contributions to the partition function.[22] We find that vibrational frequency of Te$_2$ is 257.5 cm^{-1}, in good agreement with the experimental value 246 cm^{-1}.[23] Since the surface is in chemical and thermal equilibrium with the bulk and the environment, $\mu_{Cd} + \mu_{Te} = \mu^{\text{bulk}}_{\text{CdTe}}$, thus leaving a single parameter, i.e., μ_{Te}, to describe the effect of stoichiometry. The thermodynamically allowed range of the Te-chemical potential is $\mu^{\text{bulk}}_{Te} + \Delta H_{\text{CdTe}} < \mu_{Te} < \mu^{\text{bulk}}_{Te}$, where ΔH_{CdTe} is the formation enthalpy of bulk CdTe and $\mu^{\text{bulk}}_{Te} = -3.81$ eV is the chemical potential of the bulk trigonal Te. We find that $\Delta H_{\text{CdTe}} = -0.72$ eV, in good agreement with the theoretical value of -0.76 eV[24] and the experimental value of -0.96 eV.[25] Above (below) the maximum (minimum) Te chemical potential, the Te (Cd) atoms will condense on the surface.

III. RESULTS AND DISCUSSION

In Fig. 2 we display the relative surface energy per surface area of the various reconstruction configurations relative to that of the "ideal" unreconstructed (1×1) structure as a function of $\Delta\mu_{Te} = \mu_{Te} - \mu^{\text{bulk}}_{Te}$. The thermodynamically allowed range of $\Delta\mu_{Te}$ is between the dashed blue vertical lines. We also show in the upper abscissa the dependence on temperature (upon converting μ_{Te} into temperature) at the Te vapor pressure of 3×10^{-7} and 3×10^{-6} Torr, respectively. We find that over the entire range of the allowed Te chemical potential the (2×2) Cd-vacancy reconstruction is energetically favorable over all other structures, consistent with experiment.[8–10] An

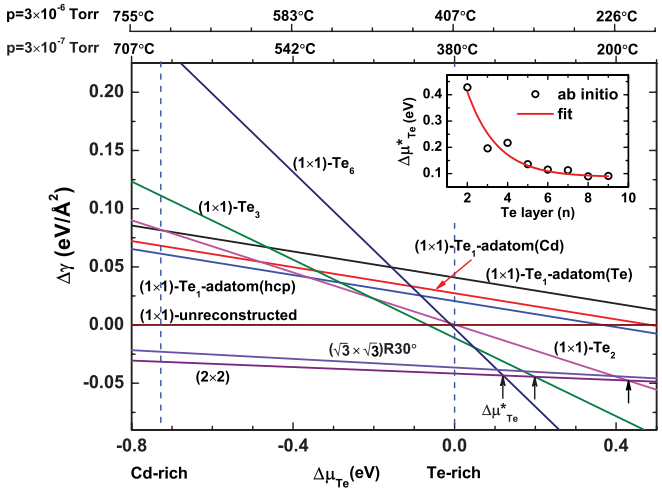

FIG. 2. (Color online) Surface free energy of the various reconstructions of the CdTe (111) A surface relative to that of the unreconstructed (1 × 1) surface versus $\Delta\mu_{Te} = \mu_{Te} - \mu_{Te}^{\text{bulk}}$. The dashed vertical lines denote the thermodynamically allowed range of μ_{Te}. The upper abscissa displays the dependence on temperature at $p_{Te} = 3 \times 10^{-7}$ and 3×10^{-6} Torr, respectively. Inset shows the *ab initio* calculated (open circles) $\Delta\mu^*_{Te}$ for the (1 × 1)-Te$_n$ → (2 × 2) transition versus the number of Te adlayers. The red curve is an exponential fit to the points.

interesting point worth noting is that we predict that the surface energy of the $(\sqrt{3} \times \sqrt{3})$R30° structure is ≈8.53 meV/Å^2 (5.14 meV/Å^2) higher than that of the (2 × 2) reconstruction in the Cd-rich (Te-rich) region, suggesting that Zn alloying may be responsible for the $(\sqrt{3} \times \sqrt{3})$R30° reconstruction observed in the $Cd_{0.96}Zn_{0.04}Te$ (111) A surface.

On the other hand, in the $\Delta\mu > 0$ Te-rich regime, the calculations reveal a series of transitions from (1 × 1)-Te$_n$→ (2 × 2) with increasing temperature, demonstrating the formation of an n-ML Te thin film at low T in agreement with experiment.[9,10] The absence of a Te adlayer in some experiments[12,13] presumably is due to the higher energy of the Ar^+ sputtering beam, which in turn removes Te adlayers. As the number of condensing Te ML increases in the Te-rich region, the (1 × 1)-Te$_n$ → (2 × 2) transition occurs at lower $\Delta^*\mu_{Te}$ values (denoted by vertical arrows) and hence higher temperatures for a given value of Te vapor pressure. Nevertheless, the thickness of the Te thin film adlayer and its dependence on temperature and/or pressure remains an open experimental question thus far.

In order to elucidate the thickness dependence of the Te adlayer on T and p, the inset of Fig. 2 displays the *ab initio* calculated (open circles) $\Delta\mu^*_{Te}$ for the (1 × 1)-Te$_n$ → (2 × 2) transition as a function of the number n of Te adlayers, which have been fitted (red curve) to $\Delta\mu^*_{Te}(T,p) = \Delta\mu^*_{Te}(n = \infty) + Ae^{-Bn}$. We find $A = 1.24$ eV, $B = 0.67$, and $\Delta\mu^*_{Te}(n = \infty) = 0.087$ eV. However, this $\Delta\mu^*_{Te}(n = \infty)$ value is higher than the 0 eV value for bulk Te, due to the presence of the CdTe-Te interface and the associated strain due to the mismatch (∼4%) of the in-plane lattice constant between the Te$_n$ adlayer and the trigonal bulk Te crystal structure. Thus, we predict that $n(T,p) = -(1/B)ln[(\Delta\mu^*_{Te}(T,p) - \Delta\mu^*_{Te}(n = \infty))/A]$, which combined with Eq. (2) yields the temperature and pressure dependence of the thickness of the absorbed Te film. For example, at $p = 3 \times 10^{-7}$ Torr if the (1 × 1)-Te$_n$ → (2 × 2) transition temperature is $T = 280$ °C, the above expression yields $n = 3.17$, corresponding to the (1 × 1)-Te$_3$ reconstruction.

TABLE I. Values of the lattice constant, a (Å), formation enthalpy of bulk CdTe, ΔH_{CdTe} (eV), and the difference in surface free energy (meV/Å^2), $\delta\tilde{\gamma} \equiv \gamma_{(\sqrt{3}\times\sqrt{3})R30^\circ} - \gamma_{(2\times2)}$, between the $(\sqrt{3} \times \sqrt{3})$R30° and (2 × 2) structures under Cd-rich and Te-rich growth conditions, employing different exchange-correlation functionals. We also list the corresponding experimental values.

	LDA	LDA + U ($U^{\text{eff}}_{Cd} = 5$ eV)[a]	PBE	Exp.
a_{CdTe}	6.421	6.409	6.629	6.481[b]
ΔH_{CdTe}	−0.72	−0.83	−0.93	−0.96[c]
$\delta\tilde{\gamma}_{Cd\text{-rich}}$	8.53	9.57	9.17	
$\delta\tilde{\gamma}_{Te\text{-rich}}$	5.14	5.96	5.10	

[a]Reference 28
[b]Reference 29
[c]Reference 25

In order to test the robustness of the relative stability of the various reconstructions with respect to the type of exchange-correlation functional used, we have also carried calculations employing the Perdew-Burke-Ernzerhof (PBE)[26] and LDA + U[27] functionals for the (2 × 2) and $(\sqrt{3} \times \sqrt{3})$R30° structures. The LDA + U formalism accounts for the strong on-site Coulomb repulsion, $U^{\text{eff}}_{Cd} = 5$ eV, amongst the localized Cd $4d$.[28] On the other hand, the relative stability of the low-temperature (1 × 1)-Te$_n$ structures is independent of the type of exchange-correlation functional as the number n of Te adlayers increases. Table I lists values of the lattice constant, formation enthalpy, and difference in surface free energy, $\delta\tilde{\gamma} \equiv \gamma_{(\sqrt{3}\times\sqrt{3})R30^\circ} - \gamma_{(2\times2)}$, between the $(\sqrt{3} \times \sqrt{3})$R30° and (2 × 2) structures, under Cd-rich and Te-rich growth conditions, employing different exchange-correlation functionals. The results demonstrate that even though different functionals yield a shift in $\Delta\gamma$ and an error in ΔH_{CdTe} of ≈0.2 eV, the relative stability of the various reconstructions remains (within 1 meV/Å^2) robust and do not affect any of the physical conclusions drawn.

In Figs. 1(a) and 1(b) we show the side and top views of the relaxed (2 × 2) reconstruction, respectively, which has one quarter of surface Cd atoms missing (white dashed circle). The remaining three quarters of the surface Cd atoms "sink" towards the adjacent Te layer by 0.86 Å, and they buckle with the same number of Te atoms in the atomic layer immediately below the surface, which in turn relax outward by 0.069 Å. This in turn leads to the formation of distorted hexagonal rings between the nearest-neighbor (NN) Cd and Te atoms with a bond length (angle) of 2.71 Å (101.14°). The remaining one quarter of Te atoms in the subsurface layer relax outward by 0.047 Å forming bonds with their NN Cd atoms of 2.83 Å and bond angle of 119.96°, thus rendering the surface bilayer almost atomically flat. This is accompanied by a lateral relaxation of the threefold coordinated Te atoms towards the Cd vacancy with a nearest-neighbor distance of

4.0 Å compared to their unrelaxed value of 4.54 Å. The second bilayer of Cd atoms is about 2.8 Å below the first bilayer with bond angles between the in- and out-of-plane NN Cd-Te bonds close to and far from the vacancy of 86.37° and 90.95°, respectively.

In Figs. 1(c) and 1(d) we show the side and top views of the relaxed (1×1)-Te_3 reconstruction, respectively, which is stable at low temperature. Interestingly we find that the three Te atoms on successive atomic layers form spiral chains on a hexagonal lattice which are oriented perpendicular to the (111) Cd-terminated surface. The NN intrachain bond lengths, $l_{12} = 2.96$ Å and $l_{23} = 3.04$ Å (where the $i, j = 1$–3 subscripts refer to the Te adlayers), are close to the corresponding value of 2.90 Å in bulk trigonal Te. Similarly, the in-plane lattice constant of the (1×1)-Te_3 CdTe (111) surface of ∼4.54 Å is very close to the experimental value of 4.45 Å of the trigonal bulk Te crystal structure.[30] These results demonstrate that under Te-rich conditions and at low temperatures a thin Te adlayer of trigonal structure is formed on the CdTe (111) A surface.

In Figs. 1(e) and 1(f) we display the top and side views of the $(\sqrt{3} \times \sqrt{3})$R30° reconstruction, respectively, which has one third of surface Cd atoms missing. Similarly with the (2×2) reconstruction, the three surface Cd (Te) atoms on the surface (subsurface) of the first bilayer relax inward (outward) by ∼0.86 Å (0.056 Å) rendering the surface almost planar. In addition, the lateral relaxation of the three Te atoms towards the Cd vacancy leads to a decrease of the NN Te-Te bond length from the ideal value of 4.54 Å to 4.1 Å, and to in-plane Cd-Te bond angles of 120° and 110.74°, respectively. The Cd atoms of the second bilayer relax outward by ∼0.072 Å leading to an interlayer distance of 2.77 Å between the first and second bilayer, and an out-of-plane bond angle of 87.67° between the in- and out-of-plane NN Cd-Te bonds.

In order to compare with recent high-resolution STM images[13] of the (2×2) reconstruction, employing the Tersoff-Hamann approach[31] we have calculated STM images of electronic charge density integrated over an energy range between the valence band maximum $E_{\rm vbm}$ and $E_{\rm vbm} + eV_b$, where V_b is the bias voltage applied to the sample with respect to the tip. The filled-state image at 2 Å above the surface under a −2 V bias in Fig. 3(a) exhibits bright rows centered on the Te surface atoms along the <110> directions, while the dark features at the vertices of the rhombus correspond to Cd vacancies centered at the threefold-coordinated Te atoms, in good agreement with the STM images.[13] Note that the intensity of the bright features associated with the three Te surface atoms

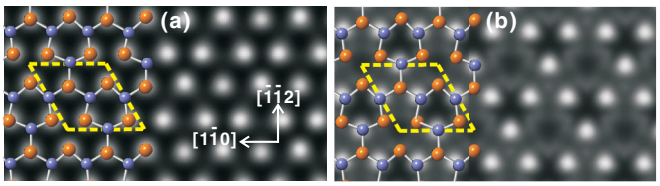

FIG. 3. (Color online) Calculated STM image of the (2×2) reconstruction of CdTe (111) A surface under (a) −2.0 V and (b) +2 V bias, respectively. The blue (red) circles denote the Cd (Te) atoms, and the vertices of the rhombus correspond to Cd vacancies at the centers of threefold coordinated Te atoms.

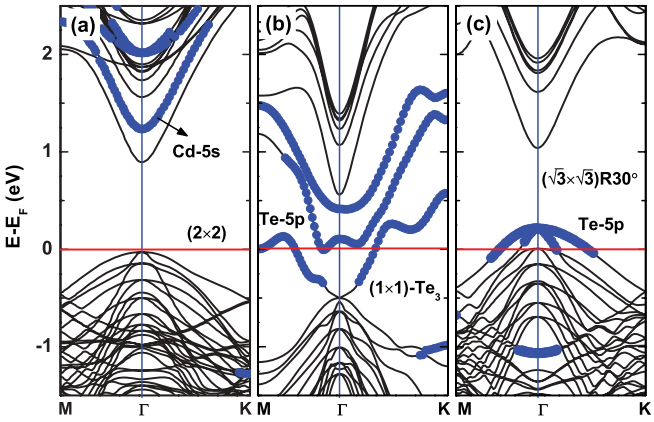

FIG. 4. (Color online) Band structure of the (a) (2×2), (b) (1×1)-Te_3, and (c) $(\sqrt{3} \times \sqrt{3})$R30° reconstructions of the (111) CdTe A surface along the symmetry directions in the two-dimensional BZ zone. The blue symbols denote surface states.

surrounding the Cd vacancy is higher than that of the Te atom not associated with the vacancy due to the fact that the latter Te atom is ∼0.02 Å lower than the other three Te atoms. On the other hand, the empty-state image in Fig. 3(b) under a +2 V bias shows bright (light gray) spots centered on the Cd (Te) surface atoms on the distorted hexagonal rings. These results are consistent with the *electron counting* (EC) rule, where the three dangling bonds on both Cd and Te surface atoms share equally their electrons resulting in completely filled (empty) dangling bonds of the more electronegative (electropositive) Te (Cd) atoms.

The band structure of the (2×2), (1×1)-Te_3, and $(\sqrt{3} \times \sqrt{3})$R30° reconstructions relative to the Fermi energy are shown in Figs. 4(a), 4(b), and 4(c), respectively, along the symmetry directions in the two-dimensional BZ, where the blue symbols denote surface states. The (2×2) configuration which satisfies the EC rule is semi-insulating with a band gap of 0.91 eV. The lower conduction band states are primarily of Cd $5s$ character with a small Te $5p$ admixture, which is in turn reflected in the STM image in Fig. 3(b). In sharp contrast, both the (1×1)-Te_3 and the $(\sqrt{3} \times \sqrt{3})$R30° reconstructions do not satisfy the EC rule and are metallic, with primarily Te $5p$-derived valences bands crossing the Fermi energy.

IV. CONCLUSION

In conclusion, we have demonstrated that the Cd-vacancy (2×2) reconstruction is the most stable structure of the Cd-terminated CdTe (111) polar surface. We predict that under Te-rich growth conditions the high-temperature semiconducting (2×2) structure undergoes a transition into the low-temperature metallic (1×1)-Te_n spiral trigonal structure. The *ab initio* thermodynamics calculations have resolved the existing open question of the temperature- and pressure-dependence of the thickness of the Te adlayer. The relative stability of the various reconstructions is robust with respect to the type of exchange correlation functional. The calculated STM images are in good agreement with experiment. The predicted small energy difference between the $(\sqrt{3} \times \sqrt{3})$R30° and (2×2) structures suggests that the underlying origin of

the experimentally observed $(\sqrt{3} \times \sqrt{3})$R30° reconstruction in the $Cd_{0.96}Zn_{0.04}Te$ (111) A surface may be due to the surface Zn-induced alloying, currently under investigation.

ACKNOWLEDGMENTS

The research at CSUN and Sivanathan Laboratories was supported by Grant No. HDTRA1-10-1-0113.

[1] Z. Zanio, *Cadmium Telluride, Semiconductors and Semimetals*, Vol. 13 (Academic Press, New York, 1978).
[2] M. Carmody, S. Mallick, J. Margetis, R. Kodama, T. Biegala, D. Xu, P. Bechmann, J. W. Garland, and S. Sivananthan, Appl. Phys. Lett. **96**, 153502 (2010).
[3] T. E. Schlesinger, J. E. Toney, H. Yoon, E. Y. Lee, B. A. Brunett, L. Franks, and R. B. James, Mater. Sci. Eng. R. **32**, 103 (2001).
[4] Y. Chang, C. H. Grein, J. Zhao, C. R. Becker, M. E. Flatte, P.-K. Liao, F. Aqariden, and S. Sivananthan, Appl. Phys. Lett. **93**, 192111 (2008).
[5] B. A. Bernevig, T. L. Hughes, and Shou-Cheng Zhang, Science **314**, 1757 (2006).
[6] A. Roth, C. Brüne, H. Buhmann, L. W. Molenkamp, J. Maciejko, X.-L. Qi, and S.-C. Zhang, Science **325**, 294 (2009).
[7] C. Szeles, Phys. Status Solidi B **241**, 783 (2004).
[8] C. Hsu, S. Sivananthan, X. Chu, and J. P. Faurie, Appl. Phys. Lett. **48**, 908 (1986).
[9] Y. S. Wu, C. R. Becker, A. Waag, M. M. Kraus, R. N. Bicknell-Tassius, and G. Landwehr, Phys. Rev. B **44**, 8904 (1991).
[10] Y. S. Wu, C. R. Becker, A. Waag, K. von Schierstedt, R. N. Ricknell-Tassius, and G. Landwehr, Appl. Phys. Lett. **62**, 1510 (1993).
[11] B. J. Kowalski, B. A. Orłowski, and J. Ghijsen, Appl. Surf. Sci. **166**, 237 (2000).
[12] J. Gordon, P. Morgen, H. Shechter, and M. Folman, Phys. Rev. B **52**, 1852 (1995).
[13] C. K. Egan, Q. Z. Jiang, and A. W. Brinkman, J. Vac. Sci. Technol. A **29**, 011021 (2011).
[14] G. Q. Zha, W. Q. Jie, T. T. Tan, P. S. Li, W. H. Zhang, and F. Q. Xu, Chem. Phys. Lett. **427**, 197 (2006).
[15] J. E. Northrup, Phys. Rev. Lett. **62**, 2487 (1989).
[16] K. Reuter and M. Scheffler, Phys. Rev. B **65**, 035406 (2001).
[17] G. Kresse and J. Furthmüller, Phys. Rev. B **54**, 11169 (1996).
[18] P. E. Blöchl, Phys. Rev. B **50**, 17953 (1994).
[19] D. M. Ceperley and B. J. Alder, Phys. Rev. Lett. **45**, 566 (1980).
[20] H. J. Monkhorst and J. D. Pack, Phys. Rev. B **13**, 5188 (1976).
[21] J. P. Gailliard, Revue Phys. Appl. **22**, 457 (1987); T. Colin and T. Skauli, J. Electron. Mater. **26**, 688 (1997).
[22] Y. Kangawa, T. Ito, Y. S. Hiraoka, A. Taguchi, K. Shiraishi, and T. Ohachi, Surf. Sci. **507**, 285 (2002).
[23] P. Hassanzadeh, C. Thompson, and L. Andrews, J. Phys. Chem. **96**, 8246 (1992).
[24] S. H. Wei and S. B. Zhang, Phys. Rev. B **66**, 155211 (2002).
[25] *CRC Handbook of Chemistry and Physics*, 88th ed., edited by D. R. Lide (CRC Press/Taylor and Francis, Boca Raton, FL, 2008).
[26] J. P. Perdew, K. Burke, and M. Ernzerhof, Phys. Rev. Lett. **77**, 3865 (1996).
[27] S. L. Dudarev, G. A. Botton, S. Y. Savrasov, C. J. Humphreys, and A. P. Sutton, Phys. Rev. B **57**, 1505 (1998).
[28] S. Lalitha, S. Zh. Karazhanov, P. Ravindran, S. Senthilarasu, R. Sathyamoorthy, and J. Janabergenov, Physica B **387**, 227 (2007).
[29] *Numerical Data and Functional Relationships in Science and Technology*, edited by K.-H. Hellwege and O. Madelung, Landolt-Börnstein, New Series, Group III, Vols. 17a and 22a (Springer, New York, 1982).
[30] R. Keller, W. B. Holzapfel, and Heinz Schulz, Phys. Rev. B **16**, 4404 (1977).
[31] J. Tersoff and D. R. Hamann, Phys. Rev. B **31**, 805 (1985).